Available online at www.sciencedirect.com

ScienceDirect

Solar Energy 124 (2016) 143–152

SOLAR ENERGY

www.elsevier.com/locate/solener

Light absorption in perovskite solar cell: Fundamentals and plasmonic enhancement of infrared band absorption

Liyang Yue *, Bing Yan, Matthew Attridge, Zengbo Wang *

School of Electronic Engineering, Bangor University, Dean Street, Bangor, Gwynedd LL57 1UT, UK

Received 19 September 2015; received in revised form 24 November 2015; accepted 26 November 2015

Communicated by: Associate Editor Frank A. Nüesch

Abstract

Perovskite solar cells have attracted great attention in recent years due to its advantageous features including low production cost, ease of fabrication and rapidly-improving device efficiencies. Research activities have been mainly devoted to the development of new manufacturing processes, materials, device structures and better stability. There is little research on the fundamentals of solar-spectrum absorption in the device layers and almost no attempts have been made to optically improve the weak absorption of perovskite materials in infrared (IR) bands. Using a full-wave simulation approach, we report for the first time the contributions of each device layers in light absorptions across the whole solar spectrum. It is found that perovskite layer dominants the absorption in UV and visible bands, while the electrode layers dominants the IR bands. In order to optically enhance the light absorption in perovskite layer in IR band, we propose to use closely-spaced plasmonic nanoparticle array to achieve considerable optical absorption in the IR band, which haven't been investigated in the literature. The concept is to use plasmonics to create hot spots in active layers, which can considerably enhance the localized light absorption in perovskite material via light-flow-circulating and nonlinear absorption mechanisms. Under optimized conditions, a 58.2% IR-band absorption enhancement has been achieved in this study. This work provides a new path towards achieving higher efficiency perovskite solar cells.

Keywords: Perovskite; Solar cell; Nanoparticle array; FIT

1. Introduction

The conversion of light into electricity is known as the photovoltaic effect, and the first solid state organo-metal halide perovskite solar cell that utilised this effect were invented in 2009 and with power conversion efficiency (PCE) of only 3.8% (Kojima et al., 2009), and then huge potential of perovskite solar cell was discovered by Kim et al. (2012) who sharp raised PCE to over 9% and attracted more researchers' interests on this topic. After 3 years development PCE figure of perovskite solar cell has been increased by 5 times more than that when it was invented and maximised to 20.1% reported by Seok et al., from the Korea Research Institute of Chemical Technology (KRICT) in 2014 and confirmed by the U.S. National Renewable Energy Laboratory (NREL) (Zimmermann et al., 2014). Perovskite's high absorption coefficient and long charge carrier diffusion length efficiently function for charge transport in the solar cell devices, and recent PCE improvement is achieved mainly by increase of efficiency of photon-electric conversion via delicate design of device to enhance material performance

* Corresponding authors. Tel.: +44 1248 382265 (L. Yue). Tel.: +44 1248 382696 (Z. Wang).

E-mail addresses: l.yue@bangor.ac.uk (L. Yue), z.wang@bangor.ac.uk (Z. Wang).

http://dx.doi.org/10.1016/j.solener.2015.11.028
0038-092X/

(Xing et al., 2013) or rise of concentration and crystallinity of perovskite using more advanced production techniques (Liu et al., 2013). However, its PCEs still cannot compete with the other photovoltaic devices, such as crystalline silicon (PCE, 25%), and gallium arsenide (PCE, 28.8%) solar cells (Green et al., 2014), so far. It is known that perovskite plays the electron donor with scaffoldings in the photon-electric conversion (Jeng et al., 2013), is also an outstanding absorber for the visible light range in the solar spectrum (Grinberg et al., 2013), nevertheless high transparency of perovskite for the light in the infrared range makes it not gain energy in full band of solar spectrum, which causes low PCE compared with the other technologies (Liu et al., 2014). For this reason, improvement of infrared absorption capability of perovskite ought to be an effective method to increase the PCE of whole solar cell system, although Ag nanoparticle in perovskite layer may act as recombination centre leading to low photocurrent along with low voltage and cancel out achieved optical gain (Lim et al., 2015).

Meanwhile, plasmonic nanoparticles are particles whose electron density can couple with electromagnetic radiation of wavelengths that are far larger than the particle, which exhibit interesting scattering, absorbance, and coupling properties based on their geometries and relative positions (Eustis and El-Sayed, 2006; Zeng et al., 2013a; Steuwe et al., 2011). Matheu et al. (2008) reported that doping of plasmonic nanoparticles can elevate the optical absorption of silicon photovoltaic devices. Atwater and Polman (2010) emphasized that plasmonics improves the absorption and reduces the physical thickness of absorber layer for thin film solar cell. Chang et al. (2014) extended this field to perovskite solar cell and found that plasmonic particles accelerate the exciton generation in the perovskite layer. Liu et al. (2014) attempted to use numerical simulation to optimise the design of planar perovskite solar cell and investigate the role of each component, and concluded that PCEs have a great dependence of the thickness and defect density of perovskite layer. Also, multiple experimental attempts were performed to explore the function of plasmonic effect in perovskite solar cell recently. Hsu et al. (2015) and Lu et al. (2015) respectively investigated the plasmonic effects of Ag nanoplates and silver–gold (Ag–Au) alloy popcorn shaped nanoparticles embedded in perovskite solar cells, and both confirmed their effects on increase of PCEs. Similar core–shell Ag at TiO_2 nanoparticles were incorporated into perovskite solar cell to improve PCEs, and corresponding result and mechanism are reported by Saliba et al. (2015). However, there has been no report about numerical modelling of regularly arranged plasmonic nanoparticle array doped in perovskite layer of solar cell for increase of optical absorption despite a number of publications about doping in the acceptor layer (Zhang et al., 2014; Bi et al., 2013; Abate et al., 2015).

In this paper, a numerical model was developed. It was firstly applied to study how each device layer absorbs sun light, and then on the optimization of IR band absorption in perovskite solar cell. Fig.1(a) and (b) depicts the model. The computation was based on finite integral technique (FIT) technique (CST Microwave Studio) proposed by Weiland. It provides a universal spatial discretization scheme, applicable to various electromagnetic problems, ranging from static field calculations to high-frequency applications in time or frequency domain (Yue et al., 2012). Unlike most numerical methods, the basic idea of FIT is to apply the Maxwell's Eq. in integral form rather than the differential ones to a set of staggered grids, which always provides more flexibilities to the model (Weiland, 1996). Here the absorptions of perovskite active layer are investigated by calculation of integral power flow on the certain interfaces in a wide wavelength range from 280 nm to 2000 nm, and regarding difference of integral power flow is considered to be absorbed by material. Total absorption flux, A_{photon}, which is the ratio between the number of absorbed photons and the number of all solar photons in unit area and time (Zeng et al., 2013b), is selected as a factor to evaluate the capability of optical absorption of model, and related data for three particle sizes (20 nm diameter, 80 nm diameter and 140 nm diameter) and 5 spacing (2 nm, 10 nm, 20 nm, 30 nm and 40 nm) are summarised and compared to a reference, $A_{photon\text{-}ref}$, of no doping model for quantification of enhancement.

2. Simulation process

2.1. Geometry, materials and boundary conditions

A model of perovskite solar cell made by vapour deposition is created in this study. Typical perovskite solar cell has 5 functional layers, respectively glass cover, transparent conducting film (anode), *n*-type compact layer, perovskite absorber layer, *p*-type hole transport material (HTM) layer and cathode (Guo et al., 2014; Liu et al., 2013; Zhou et al., 2015). Our model keeps the same layout, and tetrahedral meshing for frequency domain solver is employed for more precise calculation in this case. Materials selected for each layer are based on the established literature (Guo et al., 2014) and listed in Table 1 with layers' thicknesses. Regarding optical properties (refractive index, n and extinction coefficient, k) of materials are from the data in previous publications (SCHOTT optical glass data sheets 2012-12-04; König et al., 2014; Xie et al., 2015; Devore, 1951; Gevaerts et al., 2015; Rakić et al., 1998).

These 5 layers of materials are stacked and form a sandwich-like structure, also plasmonic particle is assumed to be a single sphere in the model and placed in the centre of perovskite layer, as shown in Fig. 1(a). Current model attempts to simulate a design of a number of regular spaced Ag particles arrays doped in the perovskite layer of the solar cell, as shown in Fig. 1(b), which is achieved through periodic boundary setting in simulation software. As shown in Fig. 1(a), the boundary conditions along x and y axis is set to be 'periodic', which means the

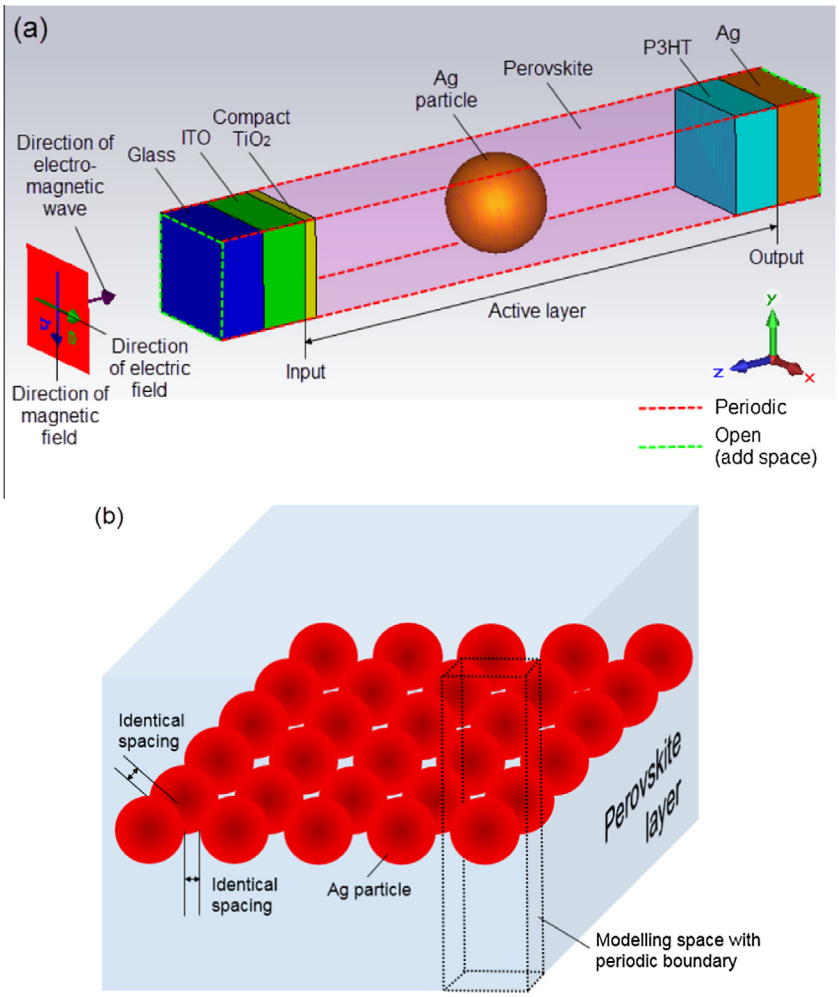

Fig. 1. (a) Model of sandwiched perovskite solar cell. (b) Diagram of simulated design of multiple particle arrays doped in perovskite layer.

Table 1
Material selection and thickness for each layer (Guo et al., 2014).

Layer name	Material	Thickness (nm)
Glass cover	Soda lime glass	40
Transparent conducting film (anode)	Indium tin oxide (ITO)	40
n-Type compact layer	TiO_2	10
Perovskite absorber layer	$CH_3NH_3PbI_3$	400
p-Type HTM layer	P3HT	40
Cathode	Silver (Ag)	40

computing boundaries at x and y direction will be simulated as that contact to the identical structure with current model and extend this repeatable pattern to the infinite space for approaching to the design of many regular particle arrays in the perovskite layer. The short dot lined area shown in Fig. 1(b) is an example to illustrate the spatial position of the model. Due to duplication of current model at the boundaries under periodic boundary conditions, computing spacing, a, is double of the distance from the particle to the boundary in current model. This horizontal spacing would be kept same on the four directions, $\pm x$ and $\pm y$. Also, boundary condition of z direction is defined as 'open (add space)' and background medium in the space is set to air due to the fact that solar cell absorbs solar electromagnetic wave from top in the normal atmosphere. As the result, it is seen that simulated electromagnetic wave (solar light) propagates towards $-z$ direction, and directions of electric and magnetic field are $-x$ and $-y$ respectively in the Fig. 1(a). Also a model representing typical perovskite solar cell without Ag particle in perovskite layer

is built under the same conditions, which demonstrates light absorption situations for normal perovskite solar cell and provides the reference data for further calculation.

2.2. Calculation of optical absorption

Energy absorption and photovoltaic effect are finished in the active layer of solar cell, which are made up by compact TiO_2 layer, perovskite layer and P3HT layer in this model, as shown in Fig. 1(a). As the target to improve of optical absorption capability, following calculation are focusing on the active layer. Our calculated wavelength range is from 280 nm to 2000 nm, which covers the highest energy band of solar spectrum. Area integral of power flow on the interfaces of active layers is calculated by CST with respect to wavelength, λ, and difference of integral power flow between input interface, P_{input}, and output interface, P_{output}, marked as 'input' and 'output' respectively in Fig. 1(a), is considered as the absorbed amount of active layer. Total absorption, $A_{(\lambda)}$, of active layer is obtained by that absorbed amount divides amount of all incident solar light, P_0, which is given by Eq. (1) (Zeng et al., 2013b):

$$A_{(\lambda)} = \frac{P_{input} - P_{output}}{P_0} \tag{1}$$

Incident power for modelling area is given by Maxwell's Eq. (2):

$$P_0 = c \cdot n \cdot \varepsilon_0 \cdot b \tag{2}$$

where c is light speed, n is refractive index of air, ε_0 is permittivity of free space, and b is the size of modelling area along z direction.

For standard solar spectrum (AM1.5), $S_{(\lambda)}$, is a curve to characterise the change of solar power flux at various wavelengths (unit W/m^2/nm), it can be transferred to solar photon flux density, $\phi_s(\lambda)$, to define as the number of photons in unit time and volume (/m^2/s) using Eq. (3) (Zeng et al., 2013b):

$$\phi_s(\lambda) = S_{(\lambda)} \cdot \frac{\lambda}{hc} \tag{3}$$

where h is the plank constant. Combining total absorption, $A_{(\lambda)}$, and solar photon flux density, $\phi_s(\lambda)$, a factor called total absorption flux, A_{photon}, is given by Eq. (4):

$$A_{photon} = \frac{\int A(\lambda)\phi_s(\lambda)d\lambda}{\int \phi_s(\lambda)d\lambda} \tag{4}$$

It is a ratio of two integral area, can evaluate the final absorption of certain layers in complete wavelength band. Larger factor means solar cell can store more photons from solar in unit area and time. Also, $A_{photon\text{-}ref}$ is total absorption flux for the no doping model, which is calculated first as reference. A_{photon} for doping models with multiple parameter combinations would be compared with it. Final percentage of absorption enhancement, $P_{enhancement}$, of plasmonic particle doping is given by Eq. (5) (Zeng et al., 2013b),

$$P_{enhancement} = \left(\frac{A_{photon}}{A_{photon-ref}} - 1\right) * 100\% \tag{5}$$

3. Results

3.1. Total absorption, $A_{(\lambda)}$

3.1.1. Model of typical perovskite solar cell without nanoparticle doping

A model of typical perovskite solar cell without plasmonic nanoparticle array doping is created to study how normal perovskite solar cell absorbs light and provide reference data for calculation of total absorption, $A_{(\lambda)}$ for afterward doping models. As shown in Fig. 1(a), solar light propagates along z direction, and pass through compact TiO_2 layer, perovskite layer and P3HT layer where solar energy will be sequentially absorbed in order of solar cell structure. As a result, $A_{(\lambda)}$ of all layers of solar cell (black short dot) and active layer (yellow short dot) and subsequent absorption proportions (area ratio) for each single layer (except glass layer) are illustrated in Fig. 2(a), and individual curves for all these single layers are shown in Fig. 2(b). Computing wavelength range is 280–2000 nm.

From Fig. 2(a), it is known that $A_{(\lambda)}$ for active layer and all layers of solar cell maintain at a high level in the ultraviolet and visible light range, and respectively maximise to 0.95 and 0.99 at 510 nm wavelength. However, a great drop is observed from 780 nm to 800 nm wavelength, which makes active layer's $A_{(\lambda)}$ down to nearly 0 after 800 nm in the calculated wavelength range (detailed data for $A_{(\lambda)}$ of active layer after 800 nm wavelength is shown in inset of Fig. 2(a)). Also, Fig. 2(a) indicates that perovskite layer absorbs majority of solar energy captured in the active layer (red area[1]), and same drop around 780 nm wavelength is also found at its single curve in Fig. 2(b). Absorption of P3HT layer (green area) is only in red–orange visible light range. Its curve has a peak reaches to 0.167 at 615 nm wavelength, but approaches to nearly 0 in the rest of calculation band. Contrarily TiO_2 layer (blue area) plays a part in ultraviolet absorption. Its curve peaks to 0.48 at 280 nm wavelength, which contributes about 57.8% ultraviolet absorption of active layer at same wavelength, and then start to drop and achieve to nearly 0 at 395 nm wavelength. ITO and Ag layer have relatively even absorption in the calculation wavelength range (as shown in Fig. 2(b)), and their peaks are in infrared range. However, as anode and cathode of solar cell, photovoltaic effect would rule out this part of light absorption.

[1] For interpretation of color in Figs. 2 and 4, the reader is referred to the web version of this article.

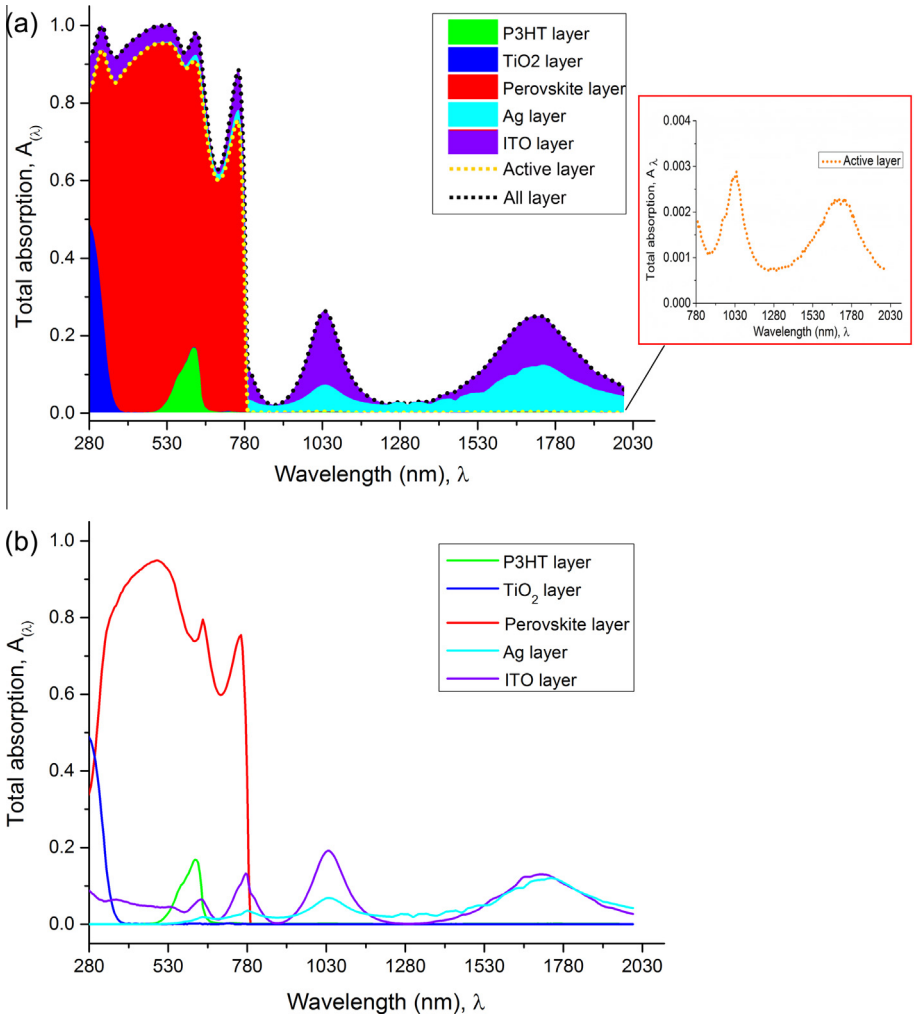

Fig. 2. (a) Total absorption, $A_{(\lambda)}$, for overall active layer in no doping structure. (b) Separate $A_{(\lambda)}$ for perovskite, P3HT and TiO_2 layer respectively in no doping structure.

3.1.2. Model with nanoparticle doping

Fig. 3(a)–(c) respectively show total absorption, $A_{(\lambda)}$ for three individual sizes of particle (diameter $D = 20$ nm, 80 nm and 140 nm) arrayed with 3 spacing ($a = 2$ nm, 10 nm, and 20 nm), and curve for active layer of no doping structure as reference is included and marked by short dot curve. The wavelength beyond 800 nm is divided into two zones (zone 1 and 2) for more convincing and clearer presentation, and shape difference between reference and doping curves are separately characterised in these two zones, whose forming mechanism are analysed in the discussion part of paper.

From Fig. 3(a), it can be seen that for 20 nm particles the profiles of curves for 3 different spacing are similar to that for reference before 780 nm wavelength, however their peaks around 770 nm are lower than that for reference except 2 nm spacing curve. Nevertheless, all doping curves do not decrease as low as reference after 780 nm wavelength though processing sharp decrease too. Slowly down gradient occurs around 790 nm wavelength for each one in the zone 1 ranged 780–1020 nm, and then create peaks in the zone 2 ranged 1020–1280 nm. It is found that 2 nm spacing has higher total absorption, $A_{(\lambda)}$, than the other curves in the zone 1 and 2, because its slowly down gradient starts from $A_{(\lambda)}$ 0.32 at 790 nm wavelength, is much higher than the 0.17 for 10 nm spacing, and 0.08 for 20 nm spacing at the same wavelength in the zone 1, and peaks to 0.60 at 1165 nm wavelength in the zone 2. Also, for models of doping of 20 nm diameter particles there is a rule characterised that heights of peaks would increase with the decline of spacing in the zone 2, meanwhile peak positions move to the longer wavelength for the shorter spacing models.

The curves representing the model of doping of 80 nm diameter particles are illustrated in Fig. 3(b). The order of curves appears shape difference in a range of 655–780 nm wavelength, which behaves several peaks higher than $A_{(\lambda)}$ 0.70 for the doping curves, but there is a trough for the reference in the same wavelength range. Then 2 nm spacing curve has an outstanding crest to 0.77 at 875 nm wavelength compared with the down trends of the other curves in the zone 1 ranged 780–1030 nm

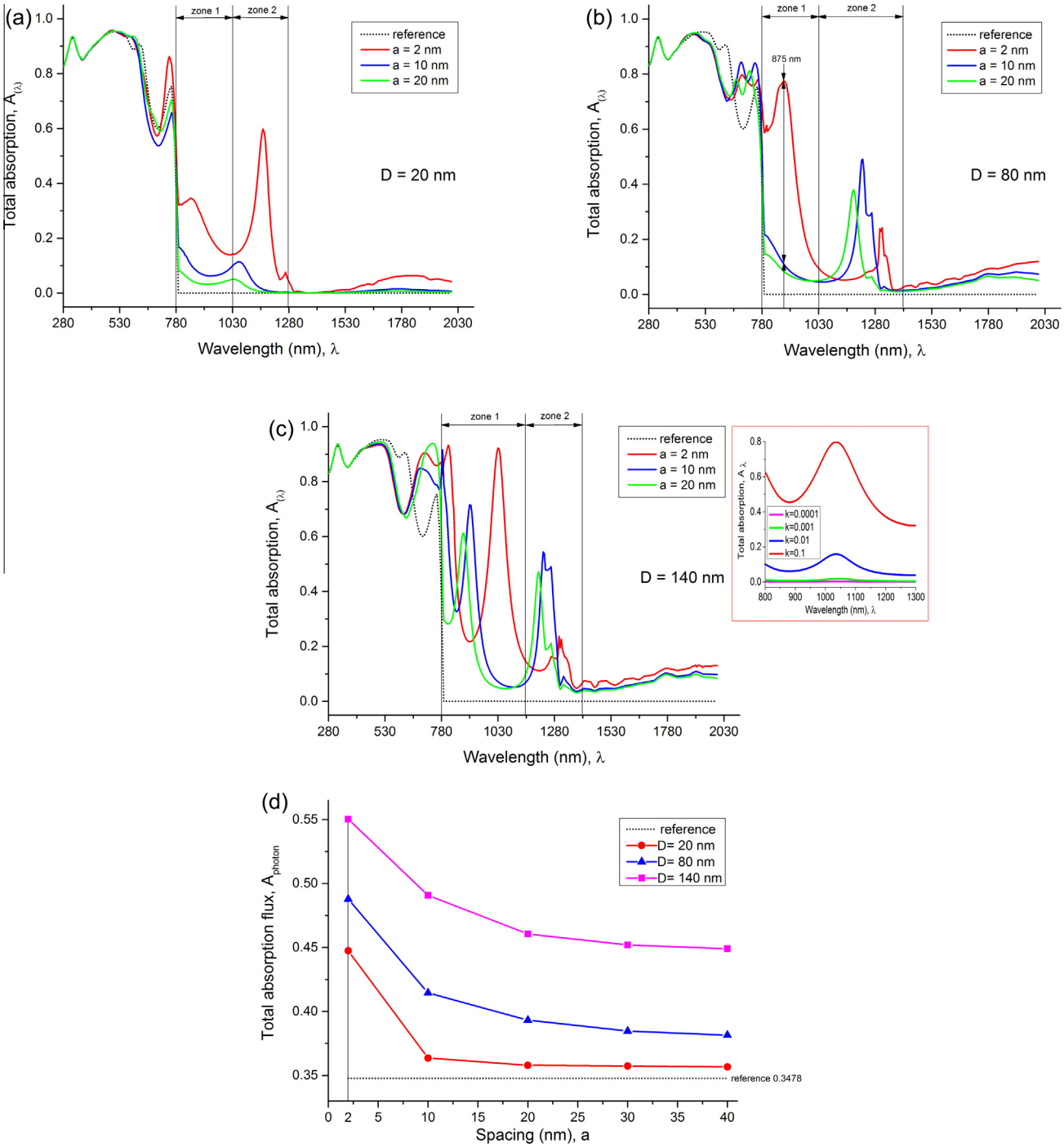

Fig. 3. Total absorption, $A_{(\lambda)}$, for (a) 20 nm diameter particle, (b) 80 nm diameter particle, (c) 140 nm diameter particle with multiple spacings, a (d) total absorption flux, A_{photon}, for parameter combinations. Short dot reference curve: model without particle doping.

wavelength in Fig. 3(b). In the zone 2 of 1020–1405 nm wavelength, generally the rule found in Fig. 3(a) still applies to the curves of doping of 80 nm diameter particles, except the peak for 2 nm spacing is not higher than that for the other curves.

$A_{(\lambda)}$ for 140 nm diameter particle is shown in Fig. 3(c). Compared with the curves of particle sized 20 nm and 80 nm diameter, model of doping of 140 nm diameter particle provides relatively high average of $A_{(\lambda)}$, and zone 1 and 2 are re-sectioned to 780–1155 nm and 1155–1405 nm wavelength respectively. Before 780 nm wavelength all curves of doping 140 nm diameter particles have a trough around 625 nm wavelength. Being different from the other particle sizes, their peaks could be seen in both zone 1 and zone 2. In zone 1, positions of peaks move forward to longer wavelength with the decline of particle spacing, and larger height is provided by smaller spacing as well as 2 nm spacing curve peaks to 0.92 at 1032 nm

wavelength. Moreover peak of 2 nm spacing is not the highest in zone 2, which is smaller than the other curves, only to 0.22 at 1310 nm wavelength.

3.2. Total absorption flux, A_{photon}

Photon flux density of solar spectrum is calculated based on the standard solar spectrum AM1.5 extracted from established literature (Collins et al., 1972; Bird et al., 1983; Gueymard, 2001). The factor, total absorption flux, A_{photon}, is the ratio between the number of absorbed photons and the number of photons irradiating to solar cell in unit area and time in fact. Due to the divergence of power distribution of solar spectrum along the wavelength, A_{photon} can effectively reflect optical absorption rate of solar cell layers at every single wavelength. A_{photon} values for parameter combinations (particle diameter and spacing) and their no doping reference are shown in Fig. 3(d). Here two more spacing ($a = 30$ and 40 nm) are included in calculation range for optimization of parameters. As reference, $A_{photon\text{-}ref}$ for no doping model approximates to 0.3478, which is marked as a short dot line in Fig. 3(d). With the same spacing larger size particle is found to provide higher A_{photon}, while smaller spacing benefits further improvement of A_{photon} for the same sized particle. Therefore, in current model highest A_{photon} is processed by 140 nm diameter particle with 2 nm spacing, and achieves to 0.5503 whose enhancement is 58.2%.

4. Discussion

4.1. Zone below 800 nm wavelength

It is well known that perovskite is an excellent absorber for the visible light in the solar spectrum (Grinberg et al., 2013), even over 0.9 absorption is observed in 'green light' wavelength range as shown in Fig. 2. The same wavelength range is also the band of solar spectrum AM1.5 providing highest energy. Hence strong absorption of visible light is considered as the main strength of the perovskite material in the solar cell. The wavelength range of sharp decline of $A_{(\lambda)}$ reference (780–800 nm) is overlapping to that for dramatic change of optical properties of perovskite material – $CH_3NH_3PbI_3$ whose extinction coefficient, k, is nearly 0 after 780 nm (Xie et al., 2015). Theoretically extinction coefficient is a factor indicates the amount of attenuation loss when the electromagnetic wave propagates through the material (Affholder and Valiron, 2001). For this reason, perovskite with $k \approx 0$ can be considered as a 'transparent' material for the infrared beyond 780 nm wavelength, which means that it is impossible to absorb solar energy in that wavelength range, and causes sharp decline of reference in 780–800 nm wavelength range, as shown in Fig. 2. If calculation range is restricted from 280 to 800 nm wavelength, total absorption flux, A_{photon}, for optimized parameter combination – 140 nm diameter particle with 2 nm spacing is 0.8502, slightly higher than reference value −0.7846. Corresponding enhancement is about 8%, which accords with the result and predicted trend between enhancement and thickness of perovskite layer reported by Carretero-Palacios et al. (2015). Therefore, in the zone of 280–800 nm wavelength, it is known that enhancement of optical absorption caused by plasmonic nanoparticle array is not as large as that in the over 800 nm wavelength range due to already existing high absorption capability of perovskite for ultraviolet and visible light.

4.2. Enhanced IR absorption Zone 1 and 2

As mentioned in 4.1, perovskite material – $CH_3NH_3PbI_3$ without particle doping only absorbs little energy ($A_{(\lambda)}$ is nearly 0) in Zone 1 and 2 (Fig. 3) band due to small extinction coefficient $k \approx 0.0001$, as shown in inset of Fig. 2(a). For this reason, majority of absorption observed in zone 1 in Fig. 3 is thought to be achieved by doping plasmonic nanoparticles, and regarding enhancement is equivalent to that for enlargement of k for 1000 times. The inset of Fig. 3(c) illustrates $A_{(\lambda)}$ for an assumed no doping model with 3 enlarged magnitudes of k values (≈0.001–10×, 0.01–100× and 0.1–1000×) within 800–1300 nm wavelength. It demonstrates that 1000 times enlarged k value −0.1 magnitude could contribute about 0.8 total absorption, $A_{(\lambda)}$ at 1030 nm wavelength, which is similar to the effect of doping of 140 nm diameter particle with 2 nm spacing shown ($A_{(\lambda)} = 0.92$ at 1032 nm wavelength) in Fig. 3(c). According to Zhang et al. (2013) except optical absorption enhancement, the doping of plasmonic nanoparticles in perovskite layer can also improve its electronic performance via increase of photoncurrent and reduction of exciton binding energy. Corresponding higher perovskite internal conversion efficiency may encourage to transfer more free electrons around plasmonic nanoparticles in perovskite layer to HTM layer.

Main physics of light interaction with spherical particles can be understood within the classic Mie theory pictures, including absorption peak and its position along the spectrum of single isolated Ag particle in the perovskite medium. In Mie theory position of absorption peak follows a rule that moving to the longer wavelength with the growth of particle size, and absorption caused by larger particle is higher than that for small particle due to less scattering. Two individual particles with short spacing would become coupled, and perform like a single larger sized particle in term of absorption and scattering under the certain frequency electromagnetic wave. Simultaneously this double particle coupling effect would be weakened if spacing is larger (Wang et al., 2004). In this case, absorption peaks for three sizes of single Ag particle are around 700 nm. Shorter spacing make the absorption peak of same sized particle move to longer wavelength direction due to double particle coupling effect, which explains why short spacing peaks are higher than that for the other spacing and close to the long wavelength. Because high absorption wavelength range of perovskite is below 780 nm and connected to zone 1,

particle absorption peaks are easy to overlap with it, only larger sized particle can effectively 'push' $A_{(\lambda)}$ curves out of strong absorption range of perovskite to the zone 1. For small sized or large spaced particles, enhancement caused by their existing is not as high as that large sized or small spaced did, however still overcomes the sharp drop of absorption in the zone 1.

It is well known that plasmonic particles can couple with electromagnetic radiation of wavelengths that are far larger than the particle due to the nature of the dielectric-metal interface between the medium and the particles (Eustis and El-Sayed, 2006). With proper spacing between particles, magnitude of electromagnetic field from solar could be enlarged in the area around particles, and regarding light flow streaming through and surrounding particles will overlap with each other in the particular areas, which form several coupling enhancement points. The field magnitude at these positions is far higher than that for the normal absorption in the medium (Wang et al., 2008). The power flow of near field for 80 nm diameter particle models with 2 nm and 10 nm spacing are simulated to be irradiated by 875 nm wavelength electromagnetic wave, as shown in Fig. 4. $A_{(\lambda)}$ for these two positions are indicated in Fig. 3 (b), and exhibit huge contrast that peak and down gradient for spacing 2 nm and 10 nm respectively. There are two different resonance modes illustrated in Fig. 4, both of them exist in the system, but respective amplitudes are depending on the size and spacing of particles. The first dominant mode is quadruple mode, which is the main status for 10 nm spacing model, as shown in Fig. 4(a). The power flow entries and leaves the particle at 4 poles, marked as red circles in Fig. 4(a), but there is no strong enhancement area between particles. All high magnitude area is in the upper part of particle. Contrarily for 2 nm spacing gap mode plays the main role in the plasmonics. The coupling resonance effectively enhances the magnitude of power flow in the gap area between two particles, which is shown as red circled area in Fig. 4(b). Carretero-Palacios et al. (2015) concluded that near-field plasmonic could boost of perovskite absorption, and resonance of particles is an important plasmonic phenomenon. Particles would resonate under a certain frequency of electromagnetic wave, and their own resonance would occur at a lower frequency than the initial electromagnetic wave. This mechanism explains the phenomenon that many peaks appear in the zone 1 and 2, and upper hand is easier to gain by gap mode with shorter spacing for same sized particle. Also, when multiple particles are short spaced, coupling effect is not only working on the particles next to each other. Coulomb's force among particles would influence their resonance (Min et al., 2013), which causes the fact that the peaks for 2 nm spacing curve in Fig. 3(b) and (c) are lower than that for other spacing curves in zone 2.

Achieved IR absorption enhancement would benefit on PCE increase of solar cell via nonlinear propagation and absorption of light power flow around plasmonic nanoparticles based on Mie theory. Basically, an interesting physics takes place in this scenario: simply straight propagation of light power flow will be replaced by complex whirl and circulate, which forms outward vortices in the host material (perovskite), and light power flows circulate the near-field areas multiple rounds (up to thousands) according this phase trajectories rather than normal one-time penetration (Bashevoy et al., 2005). For this reason, although total absorption, $A_{(\lambda)}$, of perovskite layer is only about 0.002 for wavelength over 780 nm, as shown in inset of Fig. 2 (a), this absorption can repeat thousand times and effectively promote overall PCE of perovskite solar cell. In this case, Fig. 4. shows that compared to normal situation of perovskite layer without particle doping magnitude of

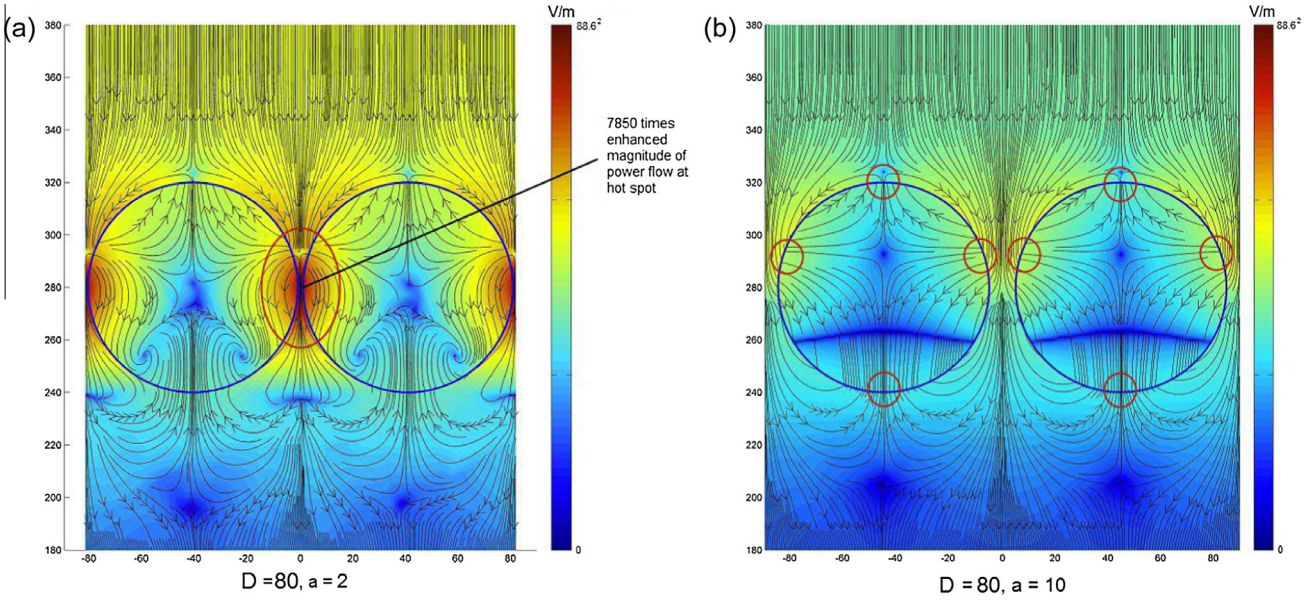

Fig. 4. Power flow diagram for 40 nm diameter particle irradiated by 875 nm electromagnetic wave with (a) 2 nm spacing and (b) 10 nm spacing.

power flow could be enhanced by 7850 times at hot spot (red circle in Fig. 4(a)) between particles with 80 nm diameter and 2 nm spacing. The nanoparticles absorbs lights via some portion of its surfaces, and then re-radiates energy via other parts of the surfaces. These flows circulates at outward vortices around particles and may form singularity points (nodes, saddle point, etc.) due to interference of scattered and incident lights. More details on flow aspects can be found in a previous publication by us (Wang et al., 2004). This light-flow-circulating effect can significantly boosted by the stronger coupling resonance initialled by smaller spacing, and few vortices found in Fig. 4(b) for larger spacing case and more power flow will be escaping in quad-pole mode (small red circles in Fig. 4 (b)) in the particle. Therefore, due to extremely high localized electric fields in hotspot zones of smaller spacing model, nonlinear propagation and absorption of IR photons is more likely to take place, rendering stronger absorption of light than previously. Also, based on this mechanism, enough space around plasmonic nanoparticle is necessary, because light power flows can adequately whirl and circulate over there while be absorbed by more perovskite in this process. As a result, ideal location of Ag nanoparticle arrays should be inside and in the middle of the perovskite layer, but then being placed on the top of perovskite layer makes against nonlinear absorption and propagation of power flow we engaged in this model and is difficult to improve optical gain in IR band.

5. Conclusion

We have explored fundamental optics behind light absorption in ordinary perovskite solar cell and concept of using closely-packed Ag nanoparticle to boost IR-band absorption. Contributions of each device layers on light absorption were first time clearly illustrated. The simulation results demonstrate that it is possible to use plasmonic Ag nanoparticles in closely-spaced form to effectively enhance the solar energy absorption in the infrared light range. A 58.2% absorption enhancement has been obtained through doping of 140 nm diameter particle arrays with 2 nm spacing. Highly localized plasmonic near-fields, with hotspots of field enhancement factor of 7850, are believed to be responsible for the observed absorption enhancement.

Acknowledgement

The authors gratefully acknowledge the financial support provided by the Sêr Cymru National Research Network in Advanced Engineering and Materials (ref: NRNF66 and NRN113).

References

Abate, A., Planells, M., Hollman, D.J., Barthi, V., Chand, S., Snaith, H.J., Robertson, N., 2015. Hole-transport materials with greatly-differing redox potentials give efficient TiO_2–$[CH_3NH_3][PbX_3]$ perovskite solar cells. Phys. Chem. Chem. Phys. 17, 2335–2338.

Affholder, M., Valiron, F., 2001. Descriptive Physical Oceanography. CRC Press, Boca Raton, FL.

Atwater, H., Polman, A., 2010. Plasmonics for improved photovoltaic devices. Nat. Mater. 9, 205–213.

Bashevoy, M.V., Fedotov, V.A., Zheludev, N.I., 2005. Optical whirlpool on an absorbing metallic nanoparticle. Opt. Expr. 13, 8372–8379.

Bi, D., Yang, L., Boschloo, G., Hagfeldt, A., Johansson, E.M.J., 2013. Effect of different hole transport materials on recombination in $CH_3NH_3PbI_3$ perovskite-sensitized mesoscopic solar cells. J. Phys. Chem. Lett. 4, 1532–1536.

Bird, R.E., Hulstrom, R.L., Lewis, L.J., 1983. Terrestrial solar spectral data sets. Sol. Energy 30, 563.

Carretero-Palacios, S., Calvo, M.E., Miguez, H., 2015. Absorption enhancement in organic–inorganic halide perovskite films with embedded plasmonic gold nanoparticles. J. Phys. Chem. C. 119, 18635.

Chang, S.H., Lin, K.F., Chiang, C.H., Chen, S.H., Wu, C.G., 2014. Plasmonic structure enhanced exciton generation at the interface between the perovskite absorber and copper nanoparticles. Sci. World J. 2014, 128424.

Collins, D.G., Blattner, W.G., Wells, M.B., Horak, H.G., 1972. Backward Monte Carlo calculations of polarization characteristics of the radiation emerging from spherical shell atmospheres. Appl. Opt. 11, 2684–2696.

Devore, J.R., 1951. Refractive indices of rutile and sphalerite. J. Opt. Soc. Am. 41, 416–419.

Eustis, S., El-Sayed, M.A., 2006. Why gold nanoparticles are more precious than pretty gold: noble metal surface plasmon resonance and its enhancement of the radiative and nonradiative properties of nanocrystals of different shapes. Chem. Soc. Rev. 35, 209–217.

Gevaerts, V.S., Koster, L.J.A., Wienk, M.M., Janssen, R.A.J., 2015. Discriminating between bilayer and bulk heterojunction polymer: fullerene solar cells using the external quantum efficiency. ACS Appl. Mater. Interfaces 3, 3252–3255.

Green, M.A., Emery, K., Hishikawa, Y., Warta, W., Dunlop, E.D., 2014. Solar cell efficiency tables (version 44). Prog. Photovoltaics 22, 701–710.

Grinberg, I., West, D.V., Torres, M., Gou, G., Stein, D.M., Wu, L., Chen, G., Gallo, E.M., Akbashev, A.R., Davies, P.K., Spanier, J.E., Rappe, A.M., 2013. Perovskite oxides for visible-light-absorbing ferroelectric and photovoltaic materials. Nature 503, 509–512.

Gueymard, C., 2001. Parameterized transmittance model for direct beam and circumsolar spectral irradiance. Sol. Energy 71, 325–346.

Guo, Y., Liu, C., Inoue, K., Harano, K., Tanaka, H., Nakamura, E., 2014. Enhancement in the efficiency of an organic–inorganic hybrid solar cell with a doped P3HT hole-transporting layer on a void-free perovskite active layer. J. Mater. Chem. A 2, 13827.

Hsu, H., Juang, T., Chen, C., Hsieh, C., Yang, C., Huang, C., Jeng, R., 2015. Enhanced efficiency of organic and perovskite photovoltaics from shape-dependent broadband plasmonic effects of Ag nanoplates. Sol. Energ. Mat. Sol. Cells 140, 224–231.

Jeng, J.Y., Chiang, Y.F., Lee, M.H., Peng, S.R., Guo, T.F., Chen, P., Wen, T.C., 2013. $CH_3NH_3PbI_3$ perovskite/fullerene planar-heterojunction hybrid solar cells. Adv. Mater. 25, 3727–3732.

Kim, H., Lee, C., Im, J., Lee, K., Moehl, T., Marchioro, A., Moon, S., Humphry-Baker, R., Yum, J., Moser, J.E., Gratzel, M., Park, N., 2012. Lead iodide perovskite sensitized all-solid-state submicron thin film mesoscopic solar cell with efficiency exceeding 9%. Sci. Rep. 2, 591.

Kojima, A., Teshima, K., Shirai, Y., Miyasaka, T., 2009. Organometal halide perovskites as visible-light sensitizers for photovoltaic cells. J. Am. Chem. Soc. 131, 6050–6051.

König, T.A.F., Ledin, P.A., Kerszulis, J., Mahmoud, M.A., El-Sayed, M. A., Reynolds, J.R., Tsukruk, V.V., 2014. Electrically tunable plasmonic behavior of nanocube–polymer nanomaterials induced by a redox-active electrochromic polymer. ACS Nano 8, 6182–6192.

Lim, S.P., Pandikumar, A., Lim, H.N., Ramaraj, R., Huang, N.M., 2015. Boosting photovoltaic performance of dye-sensitized solar cells using silver nanoparticle-decorated N, S-Co-doped-TiO_2 photoanode. Sci. Rep. 5, 11922.

Liu, M.Z., Johnston, M.B., Snaith, H.J., 2013. Efficient planar heterojunction perovskite solar cells by vapour deposition. Nature 501, 395.

Liu, F., Zhu, J., Wei, J., Li, Y., Lv, M., Yang, S., Zhang, B., Yao, J., Dai, S., 2014. Numerical simulation: toward the design of high-efficiency planar perovskite solar cells. Appl. Phys. Lett. 104, 253508.

Lu, Z., Pan, X., Ma, Y., Li, Y., Zheng, L., Zhang, D., Xu, Q., Chen, Z., Wang, S., Qu, B., Liu, F., Huang, Y., Xiao, L., Gong, Q., 2015. Plasmonic-enhanced perovskite solar cells using alloy popcorn nanoparticles. RSC Adv. 5, 11175.

Matheu, P., Lim, S.H., Derkacs, D., McPheeters, C., Yu, E.T., 2008. Metal and dielectric nanoparticle scattering for improved optical absorption in photovoltaic devices. Appl. Phys. Lett. 93, 113108.

Min, C., Shen, Z., Shen, J., Zhang, Y., Fang, H., Yuan, G., Du, L., Zhu, S., Lei, T., Yuan, X., 2013. Focused plasmonic trapping of metallic particles. Nat. Commun. 4, 2891.

Rakić, A.D., Djurišic, A.B., Elazar, J.M., Majewski, M.L., 1998. Optical properties of metallic films for vertical-cavity optoelectronic devices. Appl. Opt. 37, 5271–5283.

Saliba, M., Zhang, W., Burlakov, V.M., Stranks, S.D., Sun, Y., Ball, J.M., Johnston, M.B., Goriely, A., Wiesner, U., Snaith, H., 2015. Plasmonic-induced photon recycling in metal halide perovskite solar cells. Adv. Funct. Mater. 25, 5038–5046.

SCHOTT optical glass data sheets 2012-12-04, last accessed on 18th September 2015. <http://refractiveindex.info/download/data/2012/schott_optical_glass_collection_datasheets_dec_2012_us.pdf>.

Steuwe, C., Kaminski, C.F., Baumberg, J.J., Mahajan, S., 2011. Surface-enhanced coherent antiStokes raman scattering on nanostructured au surfaces. Nano Lett. 11, 5339.

Wang, Z.B., Luk'yanchuk, B.S., Hong, M.H., Lin, Y., Chong, T.C., 2004. Energy flow around a small particle investigated by classical Mie theory. Phys. Rev. B. 70, 035418.

Wang, Z.B., Luk'yanchuk, B.S., Guo, W., Edwardson, S.P., Whitehead, D.J., Li, L., 2008. The influences of particle number on hot spots in strongly coupled metal nanoparticles chain. J. Chem. Phys. 128, 094705.

Weiland, T., 1996. Time domain electromagnetic field computation with finite difference methods. Inter. J. Numer. Modell. 9, 295–319.

Xie, Z., Liu, S., Qin, L., Pang, S., Wang, W., Yan, Y., Yao, L., Chen, Z., Wang, S., Du, H., Yu, M., Qin, G.G., 2015. Refractive index and extinction coefficient of $CH_3NH_3PbI_3$ studied by spectroscopic ellipsometry. Opt. Mater. Expr. 5, 29–43.

Xing, G.C., Mathews, N., Sun, S.Y., Lim, S.S., Lam, Y.M., Gratzel, M., Mhaisalkar, S., Sum, T.C., 2013. Long-range balanced electron- and hole-transport lengths in organic–inorganic $CH_3NH_3PbI_3$. Science 342, 344.

Yue, L., Wang, Z., Li, L., 2012. Multiphysics modelling and simulation of dry laser cleaning of micro-slots with particle contaminants. J. Phys. D: Appl. Phys. 45, 135401.

Zeng, B., Gan, Q., Kafafi, Z.H., Bartoli, F.J., 2013a. Polymeric photovoltaics with various metallic plasmonic nanostructures. J. Appl. Phys. 113, 063109.

Zeng, S., Yu, X., Law, W.C., Zhang, Y., Hu, R., Dinh, X.Q., Ho, H.P., Yong, K.T., 2013b. Size dependence of Au NP-enhanced surface plasmon resonance based on differential phase measurement. Sensor. Actuat. B-Chem. 176, 1128.

Zhang, H., Shi, Y., Yan, F., Wang, L., Wang, K., Xing, Y., Dong, Q., Ma, T., 2014. A dual functional additive for the HTM layer in perovskite solar cells. Chem. Commun. 50, 5020–5022.

Zhang, W., Saliba, M., Stranks, S.D., Sun, Y., Shi, X., Wiesner, U., Snaith, H.J., 2013. Enhancement of perovskite-based solar cells employing core–shell metal nanoparticles. Nano Lett. 13, 4505.

Zhou, Y., Yang, M., Wu, W., Vasiliev, A.L., Zhu, K., Padture, N.P., 2015. Room-temperature crystallization of hybrid-perovskite thin films via solvent–solvent extraction for high-performance solar cells. J. Mater. Chem. A 3, 8178–8184.

Zimmermann, E., Ehrenreich, P., Pfadler, T., Dorman, J.A., Weickert, J., Schmidt-Mende, L., 2014. Erroneous efficiency reports harm organic solar cell research. Nat. Photon. 8, 669.